10-2015

Oxygen Vacancies in $LiAlO_2$ Crystals

Maurio S. Holston

I. P. Ferguson

John W. McClory
Air Force Institute of Technology

Nancy C. Giles
Air Force Institute of Technology

Larry E. Halliburton
West Virginia University

Recommended Citation

Holston, M. S., Ferguson, I. P., McClory, J. W., Giles, N. C., & Halliburton, L. E. (2015). Oxygen vacancies in LiAlO2 crystals. Physical Review B (Condensed Matter and Materials Physics), 92(14), 144108. https://doi.org/10.1103/PhysRevB.92.144108

Oxygen vacancies in $LiAlO_2$ crystals

M. S. Holston,[1] I. P. Ferguson,[1] J. W. McClory,[1] N. C. Giles,[1] and L. E. Halliburton[2,*]

[1]*Department of Engineering Physics, Air Force Institute of Technology, Wright-Patterson Air Force Base, Ohio 45433, USA*

[2]*Department of Physics and Astronomy, West Virginia University, Morgantown, West Virginia 26506, USA*

(Received 9 April 2015; revised manuscript received 17 September 2015; published 14 October 2015)

Singly ionized oxygen vacancies are produced in $LiAlO_2$ crystals by direct displacement events during a neutron irradiation. These vacancies, with one trapped electron, are referred to as V_O^+ centers. They are identified and characterized using electron paramagnetic resonance (EPR) and optical absorption. The EPR spectrum from the V_O^+ centers is best monitored near 100 K with low microwave power. When the magnetic field is along the [001] direction, this spectrum has a g value of 2.0030 and well-resolved hyperfine interactions of 310 and 240 MHz with the two ^{27}Al nuclei that are adjacent to the oxygen vacancy. A second EPR spectrum, also showing hyperfine interactions with two ^{27}Al nuclei, is attributed to a metastable state of the V_O^+ center. An optical absorption band peaking near 238 nm is assigned to V_O^+ centers. Bleaching light from a Hg lamp converts a portion of the V_O^+ centers to V_O^0 centers (these latter centers are oxygen vacancies with two trapped electrons). The V_O^0 centers have an absorption band peaking near 272 nm, a photoluminescence band peaking near 416 nm, and a photoluminescence excitation band peaking near 277 nm. Besides the oxygen-vacancy EPR spectra, a holelike spectrum with a resolved, but smaller, hyperfine interaction with one ^{27}Al nucleus is present in $LiAlO_2$ after the neutron irradiation. This spectrum is tentatively assigned to doubly ionized aluminum vacancies.

DOI: 10.1103/PhysRevB.92.144108 PACS number(s): 76.30.Mi, 61.72.jn, 78.55.Hx, 61.80.Hg

I. INTRODUCTION

Among the wide variety of oxide crystals, the oxygen vacancy is the most fundamental and extensively studied point defect. It is especially important to note the historically significant role that the oxygen vacancies have played, both experimentally and theoretically, in developing a comprehensive understanding of point defects in wide-band-gap materials [1–5]. Questions about different charge states, the nature of excited states, luminescence, lattice relaxations, formation mechanisms, etc. were addressed in a series of groundbreaking papers appearing from the late 1960s through the mid-1980s. These basic investigations initially focused on the alkaline-earth oxides, primarily MgO and CaO [6–10], and then expanded to the more complex oxides Al_2O_3 and $MgAl_2O_4$ [11–16]. Oxygen vacancies in these prototype materials continue to be the subject of advanced studies [17–28], with recent efforts also including oxides such as ZnO and TiO_2 [29–34]. The present paper extends this series of fundamental studies of oxygen vacancies to $LiAlO_2$ crystals, a relatively simple ternary oxide. These tetragonal $LiAlO_2$ crystals have a large band gap, a small degree of covalency, and are highly amenable to computational-modeling studies using advanced density functional theory (DFT) techniques.

In addition to the significant role of $LiAlO_2$ in contributing to a general understanding of the physical and electronic structure of oxygen vacancies, this material has an equally important role as a tritium breeder. Tritium is needed as a fuel for future energy-producing fusion reactors. Placing a lithium-containing compound, such as $LiAlO_2$, in the high-flux region of a present-day nuclear reactor allows thermal neutrons to produce tritium by ^{6}Li(n,α)T reactions [35]. However, it is challenging to efficiently extract the tritium from the breeder material [36–38]. One mechanism that may decrease the recoverable yield of tritium is the trapping of tritium ions at oxygen vacancies. It is well established that hydrogen, in the form of H^- or H^{2-} ions, can be stably trapped in oxygen vacancies in MgO and ZnO [39–42]. Analogous tritium-trapping behaviors are expected for oxygen vacancies in neutron-irradiated $LiAlO_2$.

In this paper, oxygen vacancies with one trapped electron (referred to as V_O^+ centers) are produced in $LiAlO_2$ crystals during an irradiation with high-energy neutrons. These V_O^+ centers are responsible for an optical absorption band peaking near 238 nm and an electron paramagnetic resonance (EPR) spectrum showing resolved hyperfine structure from the two ^{27}Al ions neighboring the vacancy. This observation of the EPR spectrum from V_O^+ centers in $LiAlO_2$ is significant, since the analogous spectrum from V_O^+ centers has proven difficult to detect in Al_2O_3 crystals [11,16] and has never been reported in $MgAl_2O_4$ crystals. Of even greater interest in this paper is the use of EPR to identify a metastable state of the V_O^+ center in $LiAlO_2$. It is proposed that this metastable state occurs because of an asymmetrical sharing of the unpaired spin between the two Al^{3+} ions neighboring the vacancy. Thus, there are two similar "ground" states that are distinguished by which Al ion has the greater unpaired spin density. One state has a slightly higher energy and is metastable. Exposing the neutron-irradiated crystal to ultraviolet light converts a few of the V_O^+ centers to V_O^0 centers, i.e., vacancies with two trapped electrons. These V_O^0 centers have an optical absorption band that peaks at 272 nm. Photoluminescence (PL) and PL excitation (PLE) bands from the V_O^0 centers peak near 416 and 277 nm, respectively. In the older literature, the V_O^0 and V_O^+ centers are referred to as F and F^+ centers.

In early studies, Auvray-Gely *et al.* [43,44] observed an optical absorption band peaking near 236 nm in electron-irradiated $LiAlO_2$ crystals. They tentatively suggested that this band could be due to F^+ centers, and they cautiously suggested that a six-line EPR spectrum was associated with these F^+ centers. As shown in the present paper, these investigators

*Larry.Halliburton@mail.wvu.edu

were correct in their suggestion of the cause of the intense ultraviolet absorption band but were not correct in their EPR assignment (they completely missed the EPR spectra from the F^+ center and the metastable F^+ center). The importance, and also the uniqueness, of the present oxygen-vacancy paper lies in the careful correlation of a comprehensive EPR analysis with a thorough optical absorption and emission characterization of the same sample. In the future, EPR is expected to continue to play a critical role in establishing the electronic structure of the ground state of oxygen vacancies in various emerging electronic and optical materials.

In addition to the oxygen vacancies, this paper shows EPR evidence for the production of doubly ionized ($S = 1/2$) aluminum vacancies during the neutron irradiation. These are defects with one hole trapped on an oxygen ion adjacent to the aluminum vacancy. The EPR spectrum [45] assigned to a hole trapped on an oxygen ion adjacent to a lithium vacancy in $LiAlO_2$ crystals was not found following the irradiation with neutrons or after a subsequent irradiation at room temperature with x rays, even though an intense EPR signal from this defect was easily produced with x rays in the as-grown samples. We suggest that the lithium vacancies initially present in the $LiAlO_2$ crystals have trapped oxygen interstitials during the neutron irradiation and thus are no longer serving as a simple trap for radiation-induced holes. A similar trapping of oxygen interstitials by isolated magnesium vacancies has been reported in neutron-irradiated MgO [46].

II. EXPERIMENTAL

Undoped single crystals of $LiAlO_2$ were obtained from the MTI Corporation (Richmond, CA). The melting point of the material is near 1700 °C and crystals are grown by the Czochralski method. Samples with dimensions of $3 \times 5 \times 0.5\,mm^3$ were cut from a larger $10 \times 10 \times 0.5\,mm^3$ [001] plate. Several samples were irradiated with neutrons at the Ohio State University Nuclear Reactor Laboratory (Columbus, Ohio). This pool-type reactor operates at a maximum power of 450 kW. One $LiAlO_2$ crystal was held in the central irradiation facility (CIF) of the reactor for 3 h, and another crystal was held in the CIF for 1.5 h. Similar spectroscopic results were obtained from the two samples (the sample receiving the larger dose of neutrons had larger concentrations of defects). At the CIF location, the total neutron flux was $\sim 2.1 \times 10^{13}$ neutrons $cm^{-2}s^{-1}$, and the thermal neutron flux was $\sim 1.3 \times 10^{13}\,cm^{-2}\,s^{-1}$. The sample temperature was not monitored during the neutron irradiations but is estimated to have remained below 150 °C.

The $LiAlO_2$ crystals have tetragonal symmetry (space group $P4_12_12$) with lattice constants $a = 5.1687$ Å and $c = 6.2679$ Å at room temperature [47]. Figure 1 is a schematic representation of this structure. The crystal consists of distorted tetrahedra with aluminum and lithium ions at the centers and oxygen ions at the vertices. Each Al^{3+} ion has four oxygen neighbors, and each Li^+ ion has four oxygen neighbors. The oxygen ions are all crystallographically equivalent and are located at the centers of distorted tetrahedra with two Al^{3+} and two Li^+ neighbors. In a particular oxygen-centered tetrahedron, the two Al-O bond lengths are 1.755 and 1.767 Å, and the two Li-O bond lengths are 1.948 and 2.059 Å. The

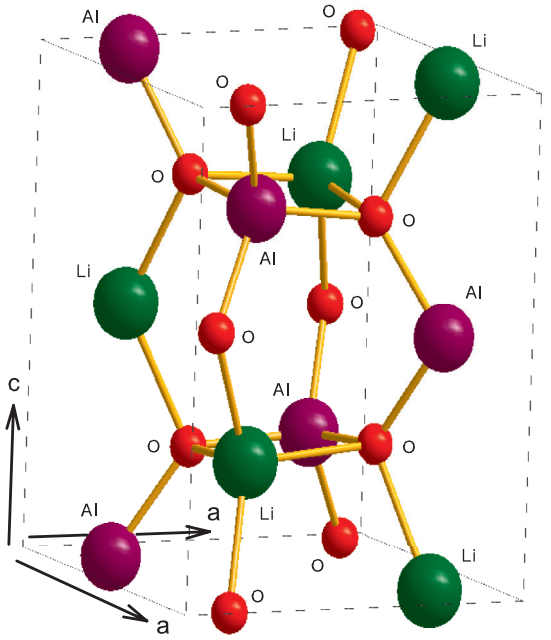

FIG. 1. (Color online) Tetragonal γ-$LiAlO_2$ crystal structure. Lithium ions are green, aluminum ions are violet, and oxygen ions are red. Each oxygen ion has two lithium neighbors and two aluminum neighbors.

optical band gap of $LiAlO_2$ is large with a transparency window extending beyond 190 nm in as-grown undoped material [48].

A Bruker EMX spectrometer operating at 9.400 GHz was used to take the EPR data. The sample temperature was controlled with a helium-gas-flow system from Oxford Instruments, and magnetic fields were measured with a Bruker nuclear magnetic resonance (NMR) teslameter. Estimates of the concentration of defects contributing to an EPR spectrum were based on comparisons to a standard pitch sample provided by Bruker. Optical absorption spectra were taken with a Cary 5000 spectrophotometer. Absorption data were corrected for surface reflection losses. Photoluminescence and PLE spectra were obtained with a Horiba Fluorolog-3 spectrometer. This spectrometer has a xenon lamp as the excitation source, a Hamamatsu R928 photomultiplier, and double-grating monochromators for selecting excitation and emission wavelengths. Slit widths for these monochromators were set for 10 nm resolution. The PL emission band was corrected for detection system response.

III. RESULTS

A. V_O^+ center EPR spectra

Figure 2(a) shows the EPR results obtained from the $LiAlO_2$ crystal after it was irradiated with neutrons for 3 h. Prior to the irradiation, only a few weak signals from transition-metal ions were observed in this field region. Two similar overlapping spectra from singly ionized oxygen vacancies are present in Fig. 2(a), as illustrated in Fig. 2(b) and 2(c). These oxygen-vacancy spectra contain large numbers of partially resolved ^{27}Al hyperfine lines of similar intensity in the magnetic field

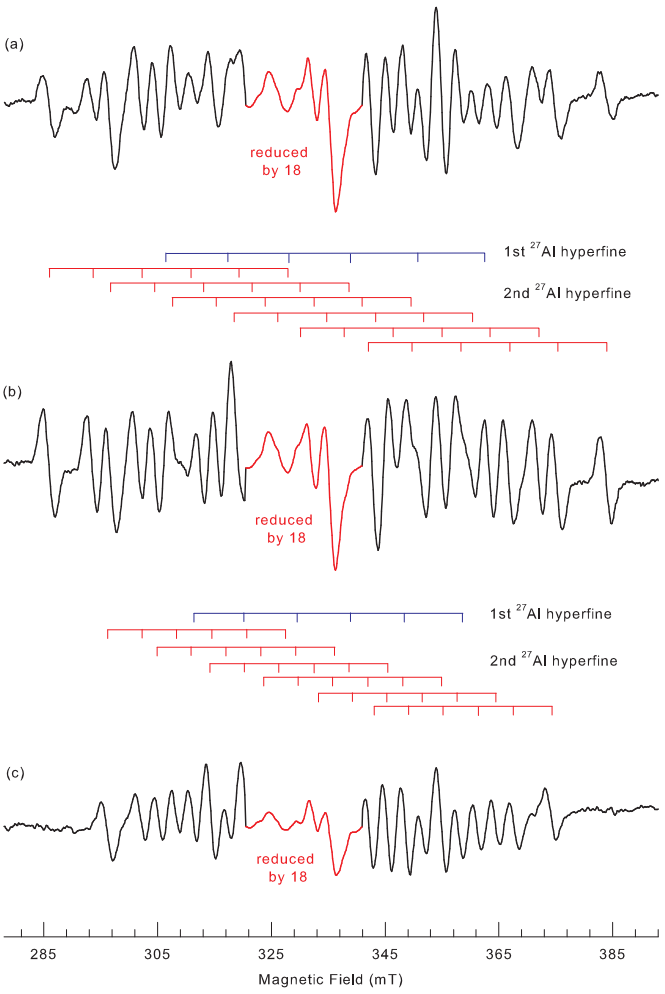

FIG. 2. (Color online) EPR spectra of oxygen vacancies in a neutron-irradiated $LiAlO_2$ crystal. Data were taken at 100 K with the magnetic field along the [001] direction. The center portion (shown in red) of each spectrum has been reduced by a factor of 18. Stick diagrams identify the hyperfine lines from the two ^{27}Al nuclei adjacent to the oxygen vacancy. (a) Spectrum with both V_O^+ and V_O^{+*} centers. (b) Spectrum of only the V_O^+ centers. (c) Spectrum of only the V_O^{+*} centers.

region extending from 284 to 384 mT. There are also three larger intensity lines between 322 and 340 mT from unrelated defects that cover up a portion of the middle lines from the oxygen vacancies. The center portions of the EPR spectra in Fig. 2 have been reduced by a factor of 18 to show these lines from the non-oxygen-vacancy defects. One of the two oxygen-vacancy spectra in Fig. 2(a) is assigned to stable V_O^+ centers, and the other is assigned to a metastable form of the V_O^+ centers (labeled V_O^{+*} centers in this paper). The EPR spectra in Fig. 2 were taken at 100 K, with the magnetic field in the [001] direction and approximately 20 μW of microwave power. Although large concentrations of oxygen vacancies are present in the neutron-irradiated crystal, their EPR spectra were not easy to observe. Individual lines from the V_O^+ and V_O^{+*} centers are broad ($\sim$2 mT), and the spectra easily saturate with microwave power. These severe microwave saturation effects make it difficult to detect the oxygen-vacancy spectra in Fig. 2 at lower temperature and higher microwave power. Each spectrum in Fig. 2 is an average of 25 scans, thus improving the signal-to-noise ratio by a factor of five.

The following steps established that two distinct oxygen-vacancy EPR spectra are present in the neutron-irradiated $LiAlO_2$. Figure 2(a) shows the spectrum taken after the irradiation. The crystal was then held at 200 °C for 1 min. It was returned to 100 K where the EPR spectrum was taken again. This spectrum, in Fig. 2(b), has resolved ^{27}Al hyperfine structure and is due entirely to the V_O^+ center (ignoring, of course, the central unrelated lines). It is apparent when comparing Figs. 2(a) and 2(b) that the widely distributed set of lines in Fig. 2(a) contains contributions from two similar defects. To identify the lines belonging to the second defect, the spectrum in Fig. 2(b) was subtracted from the spectrum in Fig. 2(a). Before performing the subtraction, the intensity of the spectrum in Fig. 2(b) was adjusted so that the intensities of the highest-field line in Figs. 2(b) and 2(a) were the same. This process resulted in the difference spectrum shown in Fig. 2(c). The broad set of EPR lines in Fig. 2(c) is due entirely to the second defect and is assigned to the V_O^{+*} center, a metastable state of the V_O^+ center. Consistent with a metastable state, the V_O^{+*} center becomes thermally unstable below 200 °C and thus is less stable than the V_O^+ center. Also, the intensity of the V_O^+ center spectrum increased when the V_O^{+*} centers were thermally destroyed, implying there was a conversion of V_O^{+*} centers to V_O^+ centers. As stated earlier, the intense lines in the middle of all three spectra in Fig. 2 (i.e., the region shown in red where the spectra are reduced by the factor of 18) are from unrelated defects and thus can be temporarily ignored (they are considered in Sec. III E). These unrelated signals have the same intensity in Figs. 2(a) and 2(b). They are still present in Fig. 2(c), although now half as intense, because the intensity of the overall spectrum in Fig. 2(b) was reduced by a factor of two before the subtraction from the spectrum in Fig. 2(a).

An oxygen vacancy in $LiAlO_2$ has four neighbors, two lithium and two aluminum ions. In the unrelaxed lattice, each of these four neighbors has a slightly different distance to the center of the oxygen vacancy. For the paramagnetic vacancy, there will be an unequal sharing of the unpaired electron among these four cations, with more of the spin density at the Al^{3+} neighbors and less of the spin density at the Li^+ neighbors. Even the two Al^{3+} ions will not have equal spin densities because of their slightly inequivalent positions and the different distances of their more distant neighboring ions from the oxygen vacancy. As expected, the V_O^+ and V_O^{+*} EPR spectra in Figs. 2(b) and 2(c) show resolved hyperfine structure from the larger interactions with adjacent ^{27}Al nuclei and no resolved hyperfine structure from the smaller interactions with adjacent ^{7}Li nuclei. (The ^{27}Al nuclei are 100% abundant with $I = 5/2$ and the ^{7}Li nuclei are 92.5% abundant with $I = 3/2$). Stick diagrams above the spectra in Figs. 2(b) and 2(c) identify the individual hyperfine lines from the two neighboring ^{27}Al nuclei. In each case, the blue lines represent the six transitions due to the larger of the two ^{27}Al interactions (referred to in Fig. 2 as the 1st ^{27}Al nucleus). Each blue line is then split into six red lines, as a result of the smaller of the two ^{27}Al interactions (referred to in Fig. 2 as the 2nd ^{27}Al nucleus). This gives 36 hyperfine lines from the two ^{27}Al interactions. There is some overlap among these ^{27}Al lines, and a few are

TABLE I. Spin-Hamiltonian parameters for the V_O^+ and V_O^{+*} centers in a neutron-irradiated $LiAlO_2$ crystal. These g and A values were obtained from the EPR spectra in Figs. 2(b) and 2(c), taken with the magnetic field along the [001] direction. Estimates of uncertainties are ±0.0005 for the g values and ±2 MHz for the A values.

	V_O^+ center	V_O^{+*} center
g	2.0030	2.0030
A_1 for 1st ^{27}Al hyperfine	310 MHz	258 MHz
A_2 for 2nd ^{27}Al hyperfine	240 MHz	182 MHz

underneath the three larger unrelated lines in the middle of the spectrum. The concentration of V_O^+ centers contributing to the spectrum in Fig. 2(b) is approximately 1.1×10^{19} cm^{-3}.

The EPR spectra of the V_O^+ and V_O^{+*} centers in Figs. 2(b) and 2(c) have very little angular dependence. Thus, each spectrum can be simply described by a g parameter and two hyperfine parameters, one for each ^{27}Al neighbor. A spin-Hamiltonian with an electron Zeeman term and two hyperfine terms was used to determine values of these parameters for each center

$$H = g\beta \mathbf{B} \cdot \mathbf{S} + A_1 \mathbf{I_1} \cdot \mathbf{S} + A_2 \mathbf{I_2} \cdot \mathbf{S}. \quad (1)$$

The comprehensive EasySpin [49] computer program was used to predict the positions of individual EPR lines for this Hamiltonian (where $\mathbf{S} = 1/2$, $\mathbf{I}_1 = 5/2$, and $\mathbf{I}_2 = 5/2$). EasySpin converts the spin Hamiltonian in Eq. (1) to a 72×72 matrix and then performs a full diagonalization to obtain the energy levels. An iterative fitting process was used to find final sets of parameters for the V_O^+ and V_O^{+*} centers. Input data were a microwave frequency and a magnetic field position for each of the three highest-field lines and three lowest-field lines in Figs. 2(b) and 2(c), respectively. Results of these fittings are given in Table I. Figure 3 shows a simulation of the V_O^+ EPR spectrum using the parameters in Table I. For ease of comparison, the experimental spectrum from Fig. 2(b) is shown again in Fig. 3(a), and the simulated spectrum is then shown in Fig. 3(b). Second-order effects due to the large hyperfine parameters cause the experimental EPR spectra to be slightly asymmetrical. For example, in the V_O^+ center spectrum in Fig. 3(a), the highest two lines near 379 mT are separated by 8.62 mT, while the lowest two lines near 289 mT are separated by 7.64 mT.

For V_O^+ centers in Al_2O_3 crystals, the measured g value is 2.0030, and the isotropic portions of the hyperfine interactions are 147.0 MHz for two of the ^{27}Al neighbors and 29.8 MHz for the other two ^{27}Al neighbors [16]. Table I shows that the g values for the V_O^+ and V_O^{+*} centers in $LiAlO_2$ are the same as the g value of the V_O^+ center in Al_2O_3. The hyperfine interactions for the two ^{27}Al neighbors of the V_O^+ and V_O^{+*} centers in $LiAlO_2$ are, however, about a factor of two larger than the corresponding values for the V_O^+ center in Al_2O_3. The differences in the ^{27}Al hyperfine parameters for the two materials may be related to the distances from the center of the oxygen vacancy to aluminum neighbors. The two closest Al^{3+} ions in Al_2O_3 are 1.855 Å from the vacant oxygen site, while Al^{3+} ions in $LiAlO_2$ are 1.755 and 1.766 Å from the vacancy. This smaller distance in $LiAlO_2$ is consistent with a larger unpaired spin density on its two Al^{3+} ions.

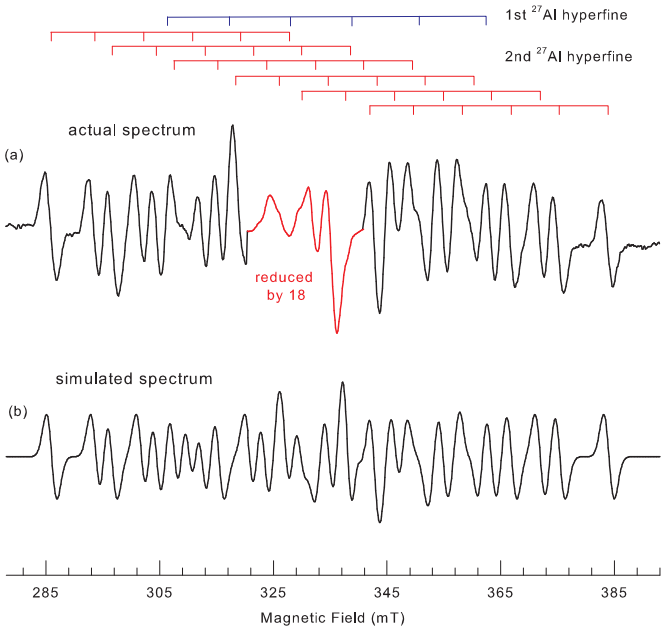

FIG. 3. (Color online) (a) Measured EPR spectrum from the V_O^+ center [this spectrum is the same as in Fig. 2(b)]. (b) Simulated EPR spectrum of the V_O^+ center using the spin-Hamiltonian parameters in Table I.

The presence in Fig. 2 of the V_O^{+*} centers, a metastable version of the V_O^+ centers, was unexpected. A plausible explanation for the coexistence of both V_O^+ and V_O^{+*} centers is related to the observed unequal sharing of the unpaired spin density by the two Al^{3+} ions adjacent to the oxygen vacancy. The EPR spectra in Figs. 2(b) and 2(c) do not specify which of the two Al^{3+} ions has the greater spin density (see Table I), nor do they provide information about the relative lattice relaxations of these two ions. It is, however, reasonable to assume that the Al^{3+} ion having a larger spin density in the V_O^+ center will have a smaller spin density in the V_O^{+*} center. This results in two distinct distributions of the unpaired spin density for the singly ionized oxygen vacancies. Each of these configurations will be accompanied by a unique relaxation of the two Al^{3+} ions and the surrounding lattice. The minimum energy of one configuration (the V_O^{+*} center) will be greater than the minimum energy of the other configuration (the V_O^+ center), and their potential wells will be separated by a potential barrier. When sufficient energy is available to overcome this barrier, the V_O^{+*} centers are able to thermally convert to V_O^+ centers, as shown in Fig. 2. In support of the arguments presented here, an earlier EPR study of defects in lithium β-alumina has reported the observation of two inequivalent V_O^+ centers [50].

B. Optical absorption

Figure 4 shows the optical absorption spectrum (blue curve) of the $LiAlO_2$ crystal taken at room temperature after a 3 h irradiation with neutrons. Unpolarized light propagated along the [001] direction in the crystal, and the path length (i.e., thickness) was 0.5 mm. The primary band in Fig. 4 has a peak near 238 nm (5.21 eV) and is assigned to the V_O^+ centers. This

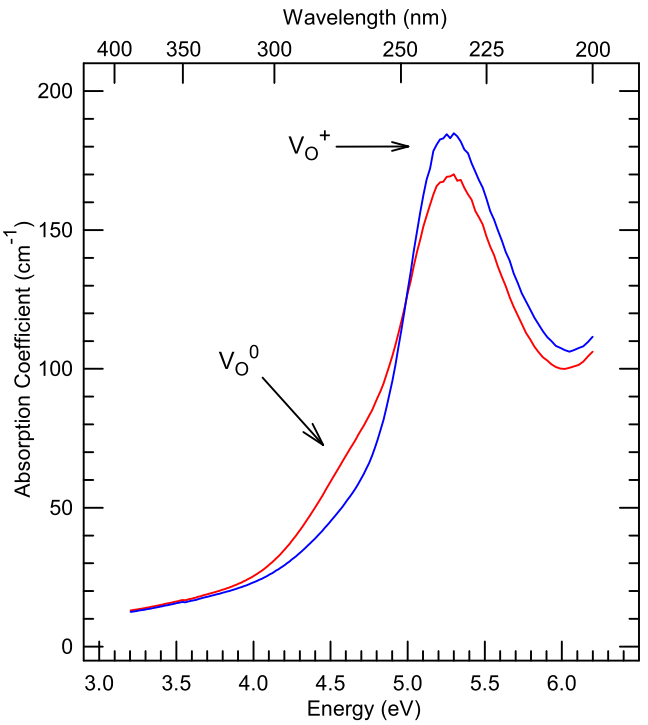

FIG. 4. (Color online) Room-temperature optical absorption spectra from a $LiAlO_2$ crystal. The blue curve was taken after the neutron irradiation. The red curve was taken after exposing the irradiated crystal to a Hg lamp. The V_O^+ band peaks near 238 nm, and the V_O^0 band peaks near 272 nm.

238 nm absorption peak was initially observed by Auvray-Gely *et al.* [43,44] in $LiAlO_2$ crystals irradiated with high-energy electrons. Evidence that the 238 nm optical absorption band is due to V_O^+ centers is provided by the thermal annealing results reported in Sec. III C.

There were no significant absorption bands in the 200–300 nm region prior to the neutron irradiation. Furthermore, an absorption band near 238 nm did not appear when as-grown crystals were irradiated at room temperature with x rays. (The x rays are unable to create oxygen vacancies through a direct momentum-conserving displacement mechanism and are only able to change the charge state of preexisting oxygen vacancies). This indicates that there are very few, if any, oxygen vacancies initially present in Czochralski-grown $LiAlO_2$ crystals. Also, the lack of an observable x-ray-induced V_O^+ center EPR spectrum before the neutron irradiation supports the absence of oxygen vacancies in the as-grown crystals. Together, these results establish that the oxygen vacancies represented by the EPR spectra in Fig. 2 and the 238 nm absorption band in Fig. 4 were produced by displacement events initiated by high-energy neutrons. As demonstrated by Auvray-Gely *et al.* [43,44], high-energy electrons can also displace oxygen ions.

By combining the EPR and optical absorption results from the same sample, a value for the oscillator strength of the V_O^+ optical band is determined. In general, the oscillator strength, designated as f, is a characteristic parameter of a defect that relates the intensity of an optical absorption band to the number of defects responsible for the absorption band. Smakula's equation [51], in the form appropriate for a Gaussian-shaped band, is used to calculate f

$$Nf = (0.87 \times 10^{17}) \frac{n}{(n^2+2)^2} \alpha_{\max} W. \quad (2)$$

The concentration N of V_O^+ centers contributing to the EPR spectrum in Fig. 2(b) is $1.1 \times 10^{19}\,cm^{-3}$. The corresponding absorption band from the same crystal is shown in Fig. 4 (blue curve). After accounting for the increasing baseline beneath this absorption band, the absorption coefficient at the peak $\alpha_{\max}$ is $135\,cm^{-1}$, and the full width at half maximum W is 0.90 eV. An estimate [52] for the index of refraction n is 1.65. Substituting these quantities into Eq. (2) gives an oscillator strength of 0.07 for the 238 nm V_O^+ center absorption band in $LiAlO_2$ crystals.

A close examination of the optical absorption spectrum taken after the neutron irradiation (the blue curve in Fig. 4) shows a weak shoulder near 272 nm (4.56 eV) on the low energy side of the primary absorption band. As illustrated by the red curve in Fig. 4, exposing the neutron-irradiated crystal at room temperature to a low-intensity Hg lamp reduces the main 238 nm band and enhances the optical absorption band at 272 nm. In a likely scenario, light from the Hg lamp releases electrons from unidentified traps (for example, Fe^+ or other transition-metal ions). These electrons are trapped by V_O^+ centers, thus converting them into V_O^0 centers. The broad, less intense, absorption band peaking near 272 nm in Fig. 4 is assigned to these V_O^0 centers. (A V_O^0 center is an oxygen vacancy with two trapped electrons). In both CaO and SrO crystals, the V_O^0 center optical absorption band occurs at a lower energy than the V_O^+ center absorption band [7,53]. The portion of V_O^+ centers that are converted to V_O^0 centers in $LiAlO_2$ by the Hg lamp is controlled by the number and types of electron traps present. After using light from the Hg lamp to increase the intensity of the 272 nm absorption band, exposing the crystal at room temperature to 325 nm light from a He-Cd laser decreased the intensity of the 272 nm band.

C. Thermal stability of the V_O^+ centers

A thermal anneal study was performed on the $LiAlO_2$ crystal that had been irradiated with neutrons for 3 h. Both the EPR spectra of the V_O^+ centers and the 238 nm optical absorption band were monitored. In these experiments, the crystal was held for 1 min at a series of progressively higher temperatures. After each anneal step, the crystal was returned to room temperature, where the optical absorption spectrum was taken, and then to 100 K, where the EPR spectrum was taken. Figure 5 illustrates the decreasing intensity of the 238 nm optical absorption band at the higher annealing temperatures. Figure 6 shows the excellent correlation of optical and EPR intensities as a function of annealing temperature, thus verifying that these spectra have a common origin. The temperature where half of the V_O^+ centers have thermally decayed is approximately 425 °C.

In Fig. 6, the blue curve represents the combined V_O^+ and V_O^{+*} intensities. At the beginning of the thermal anneal (i.e., at room temperature), both V_O^+ and V_O^{+*} centers are present in the EPR spectrum. Both of these defects are also present after

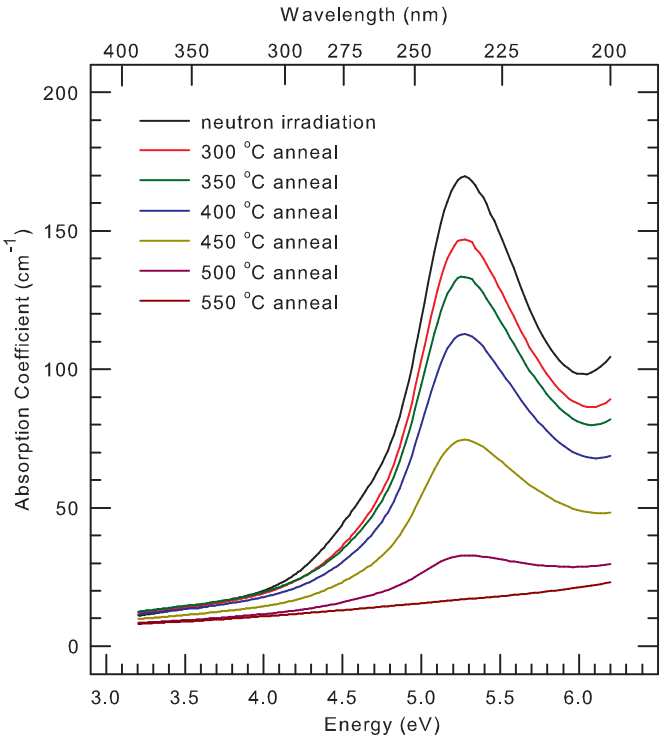

FIG. 5. (Color online) Thermal stability of the 238 nm optical absorption band assigned to V_O^+ centers. The sample was held at each temperature for 1 min and then returned to room temperature, where the absorption spectrum was recorded.

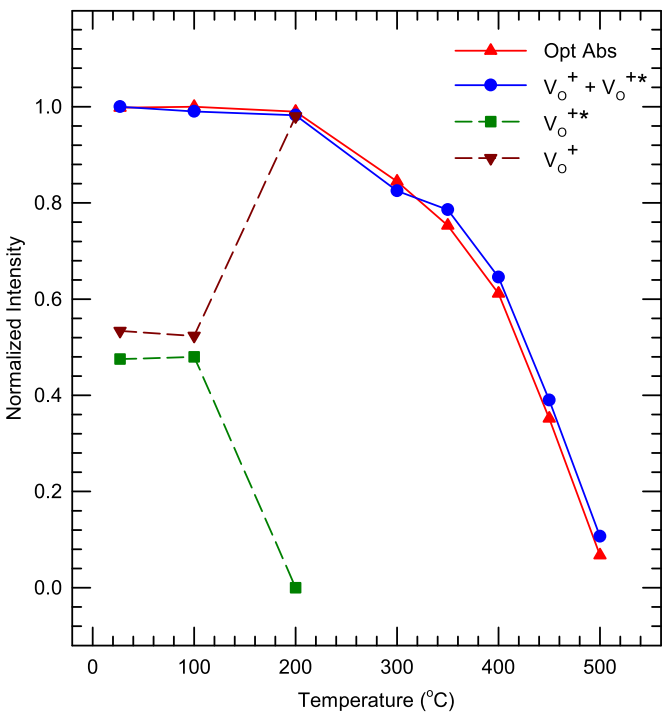

FIG. 6. (Color online) Correlation of the thermal decay of the 238 nm optical absorption band and the EPR spectrum representing the V_O^+ center. During the first annealing step, the V_O^+ and V_O^{+*} centers are both present (as indicated by the dashed green and dark red lines). The blue curve represents the total number of V_O^+ and V_O^{+*} centers.

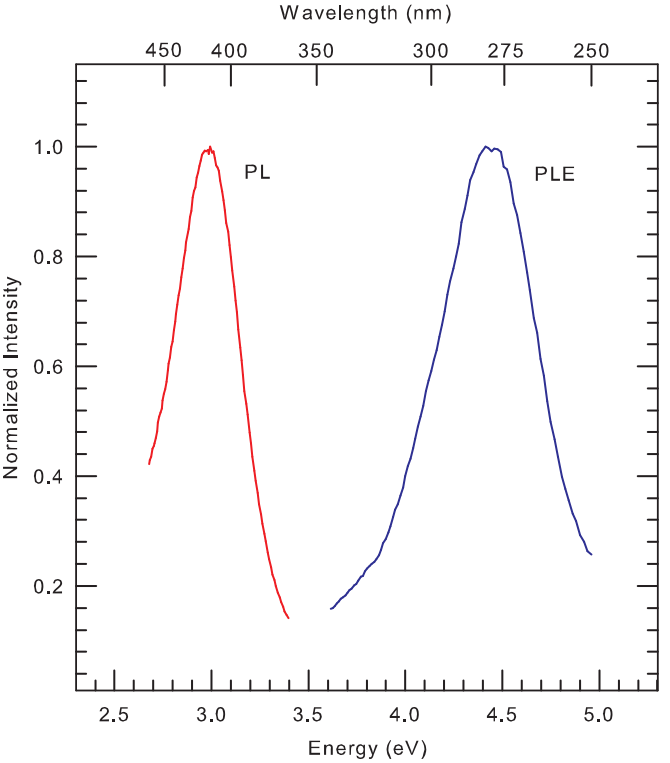

FIG. 7. (Color online) PL and PLE spectra obtained from a neutron-irradiated $LiAlO_2$ crystal. The responsible defect is the V_O^0 center.

the 100 °C anneal step. After the 200 °C anneal step, the V_O^{+*} centers have disappeared, and the intensity of the V_O^+ center EPR spectrum has increased by the amount the V_O^{+*} spectrum decreased. These effects are illustrated by the dashed lines (green and dark red) in Fig. 6 and also by the EPR spectra in Fig. 2. As described in Sec. III A, this direct thermally induced conversion of V_O^{+*} centers to V_O^+ centers strongly suggests that the V_O^{+*} centers are a metastable state of the V_O^+ centers.

D. PL and PLE from the V_O^0 center

Figure 7 shows the PL and PLE spectra taken at room temperature from the $LiAlO_2$ crystal irradiated for 3 h with neutrons. The emission band was obtained using an excitation wavelength of 300 nm. It peaks at 411 nm (3.02 eV) and has a full width at half maximum (FWHM) of 0.36 eV. The related excitation band was obtained by monitoring the emission at 410 nm. This PLE band peaks near 277 nm (4.48 eV) and has a FWHM of 0.57 eV. The resulting Stokes shift of 1.46 eV is large. Before recording the spectra in Fig. 7, the crystal was held at 300 °C for 1 min (see Sec. III C). Heating to 300 °C allowed "clean" PL and PLE spectra from a single defect to be obtained, as several interfering spectra from defect aggregates were thermally destroyed at this temperature. The PLE spectrum in Fig. 7 has been corrected for variation in excitation lamp output, and the PL spectrum has been corrected for detection system response. An additional λ^2 correction is needed when converting the PL spectrum from wavelength to energy because the emission band is broad, and a monochromator was used to select emitted wavelengths [54].

The PL peak position shifts to 416 nm (2.98 eV) when the λ^2 correction is included.

Comparison of the PLE band in Fig. 7 with the optical absorption spectra in Fig. 4 shows that the PLE band does not coincide with the V_O^+ center absorption band peaking at 238 nm (blue spectrum in Fig. 4). This lack of correlation eliminates the V_O^+ center as the defect responsible for the PL band. The peak of the PLE spectrum is, however, close to the peak of the V_O^0 center band that appears as a shoulder of the V_O^+ absorption band when the crystal is exposed to the Hg lamp (red spectrum in Fig. 4). The difference between the peak of the PLE band and the peak of the V_O^0 center band is small (272 vs 277 nm). This small difference is believed to be experimental and arises from the difficulty in identifying the peak position of the V_O^0 center absorption band in Fig. 4 and also in correcting the PLE spectrum for variations in excitation lamp intensity. This suggests that the PLE and optical absorption bands have a common origin and allows us to assign the PL and PLE spectra in Fig. 7 to V_O^0 centers.

There does not appear to be an emission band at room temperature associated with the V_O^+ center absorption band at 238 nm. Repeated attempts using excitation wavelengths between 235 and 250 nm failed to find any PL emission bands from the neutron-irradiated crystals, other than the 411 nm band in Fig. 7. Also, a preliminary search with a crystal at 77 K did not reveal any new PL band. The absence of a luminescence band associated with the V_O^+ centers in $LiAlO_2$ can be explained using the phenomenological model of Bartram and Stoneham [55]. They noted that emission is expected to be quenched when the crossover point of the excited state and ground state curves in a two-state configuration-coordinate diagram occurs below the energy reached in absorption. Their empirical relationships, based on the phonon energies and relative ionic radii, suggest that emission should not be expected from the V_O^+ centers in $LiAlO_2$ crystals.

E. EPR spectrum from the aluminum vacancy

The intense EPR lines in the middle of the spectra in Fig. 2 are shown more clearly in Fig. 8. These data are from the 3 h neutron-irradiated $LiAlO_2$ crystal. They were taken at 36 K with a microwave power of 2 mW. The magnetic field was along the [001] direction. A lower temperature and a higher microwave power were used to obtain this spectrum because the contributing defects did not easily saturate with microwave power. Also, the smaller linewidths in Fig. 8, compared to the V_O^+ center linewidths in Fig. 2, allowed a reduced modulation amplitude to be used when recording the EPR spectrum, and this in turn increased the resolution.

At least three distinct defects, and possibly more, are participating in the EPR spectrum in Fig. 8. This is not surprising since a neutron irradiation can produce paramagnetic aggregates of vacancies (e.g., dimers, trimers, etc.) as well as isolated vacancies. Also, interstitial ions may be contributing to one or more of the observed spectra. The combined concentration of the three defects is approximately the same as the V_O^+ centers in Fig. 2(b). A set of six equally spaced lines, identified by the stick diagram above the spectrum, can easily be distinguished in Fig. 8. This six-line

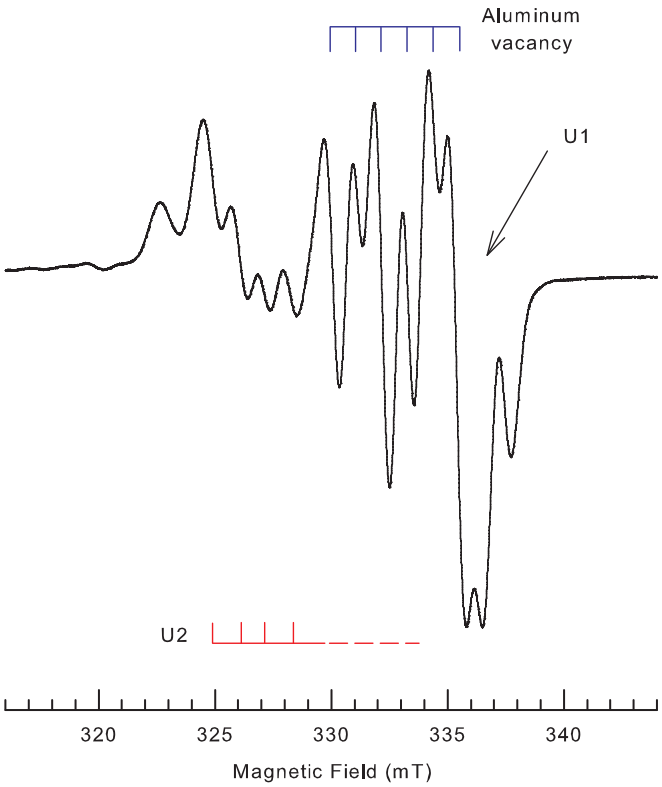

FIG. 8. (Color online) EPR spectrum from a neutron-irradiated $LiAlO_2$ crystal, taken at 36 K with high microwave power. The set of six equally spaced lines is assigned to a doubly ionized aluminum vacancy. The U1 and U2 signals have not been identified.

EPR spectrum is tentatively assigned to a doubly ionized aluminum vacancy ($S = 1/2$) produced during the neutron irradiation. In this defect, a hole (i.e., a missing electron) is trapped on an oxygen ion adjacent to the aluminum vacancy, and the six hyperfine lines are caused by the oxygen ion's one remaining neighboring ^{27}Al nucleus (100% abundant with $I = 5/2$). The six-line spectrum in Fig. 8 has very little angular dependence, thus indicating that the trapped hole may be rapidly hopping among all four of the oxygen ions adjacent to the aluminum vacancy instead of being localized on only one of the neighboring oxygen ions. Reasons for the vacancy assignment for the six-line spectrum in Fig. 8 include a holelike g value of 2.019 and a ^{27}Al hyperfine splitting parameter of 1.09 mT. These values are very similar to the g and ^{27}Al hyperfine parameters previously found for a trapped hole on an oxygen ion next to a lithium vacancy in $LiAlO_2$ crystals [45]. The defects responsible for the remaining EPR lines in Fig. 8 have not been identified. These include the single intense line, labeled U1, located near 335 mT and the set of lines, labeled U2, that extend from 324.5 mT to possibly near 335 mT. A line at low field (near 322 mT) and a line at high field (near 337.5 mT) are also unidentified.

We note with interest that the EPR lines due to trapped holes at lithium vacancies [45] are missing from the spectrum of the neutron-irradiated crystal in Fig. 8. To eliminate the possibility that the lithium-vacancy signals had thermally annealed due to inadvertent heating of the crystal during the neutron irradiation, a subsequent x-ray irradiation of the

neutron-irradiated crystal was done at room temperature. This also failed to generate the EPR signals associated with lithium vacancies. Thus, there appear to be no, or very few, isolated lithium vacancies in our neutron-irradiated $LiAlO_2$ crystals, even though large concentrations of lithium vacancies were known to be present in the as-grown crystals. Following an earlier suggestion from work in MgO [46], a possible explanation is the trapping of oxygen interstitials by lithium vacancies. Once a lithium vacancy has trapped an oxygen interstitial, it can no longer serve as a simple hole trap. Support for this interstitial-trapping mechanism comes from the following observation. After heating a neutron-irradiated $LiAlO_2$ crystal to 600 °C, a subsequent x-ray irradiation at room temperature produces an intense EPR signal from holes trapped on oxygen ions adjacent to lithium vacancies. Heating to this temperature causes all of the interstitials to recombine with oxygen vacancies (see Fig. 6). Lithium vacancies, now without a nearby oxygen interstitial, can once again trap holes on an adjacent oxygen ion (i.e., the lithium vacancies revert back to their usual hole-trapping role once the oxygen interstitials are no longer present).

IV. SUMMARY

Single crystals of $LiAlO_2$ have been irradiated with high-energy neutrons. This material serves as a prototype for studying oxygen vacancies in wide-band-gap insulators, and extends similar earlier work on MgO, Al_2O_3, and $MgAl_2O_4$ crystals. The dominant defects produced by the neutrons are oxygen vacancies with one trapped electron. These V_O^+ centers have an optical absorption band peaking at 238 nm. An EPR spectrum from these V_O^+ centers exhibits large hyperfine interactions with two neighboring ^{27}Al nuclei. Also, an EPR spectrum from a metastable state of the V_O^+ center is observed, with slightly different values for the hyperfine interactions. Optical bleaching converts V_O^+ centers to V_O^0 centers (oxygen vacancies with two trapped electrons). An emission band is seen at room temperature from the V_O^0 centers, but not the V_O^+ centers. Finally, an EPR signal from doubly ionized aluminum vacancies is present in the neutron-irradiated crystals. In these defects, a hole is trapped by one or more of the oxygen ions adjacent to the aluminum vacancy.

ACKNOWLEDGMENTS

The authors thank Susan White and Kevin Herminghuysen at the Ohio State Nuclear Reactor Laboratory for irradiating the samples and Michael Ranft and Greg Smith at the Air Force Institute of Technology for assistance with the optical measurements. Support for this paper at the Air Force Institute of Technology was provided by the Defense Threat Reduction Agency (Grants No. HDTRA1-07-1-0008 and No. BRBAA08-I-2-0128). The views expressed in this paper are those of the authors and do not necessarily reflect the official policy or position of the Air Force, the Department of Defense, or the United States Government.

[1] B. Henderson and G. F. Imbusch, *Optical Spectroscopy of Inorganic Solids* (Oxford University Press, Oxford, 1989).
[2] J. H. Crawford, Jr., Nucl. Instrum. Methods B **1**, 159 (1984).
[3] B. Henderson and J. E. Wertz, *Defects in the Alkaline Earth Oxides* (Taylor and Francis Ltd. and Halsted Press, John Wiley and Sons, NewYork, 1977).
[4] E. Sonder and W. A. Sibley, in *Point Defects in Solids: Vol. 1, General and Ionic Crystals*, edited by J. H. Crawford, Jr. and L. M. Slifkin (Plenum Press, New York, 1972), Chap. 4.
[5] A. E. Hughes and B. Henderson, in *Point Defects in Solids: Vol. 1, General and Ionic Crystals*, edited by J. H. Crawford, Jr. and L. M. Slifkin (Plenum Press, New York, 1972), Chap. 7.
[6] Y. Chen, R. T. Williams, and W. A. Sibley, Phys. Rev. **182**, 960 (1969).
[7] B. Henderson, S. E. Stokowski, and T. C. Ensign, Phys. Rev. **183**, 826 (1969).
[8] Y. Chen, J. L. Kolopus, and W. A. Sibley, Phys. Rev. **186**, 865 (1969).
[9] L. A. Kappers, R. L. Kroes, and E. B. Hensley, Phys. Rev. B **1**, 4151 (1970).
[10] B. Henderson, Y. Chen, and W. A. Sibley, Phys. Rev. B **6**, 4060 (1972).
[11] S. Y. La, R. H. Bartram, and R. T. Cox, J. Phys. Chem. Solids **34**, 1079 (1973).
[12] K. H. Lee and J. H. Crawford, Jr., Phys. Rev. B **15**, 4065 (1977).
[13] B. D. Evans and M. Stapelbroek, Phys. Rev. B **18**, 7089 (1978).
[14] K. H. Lee and J. H. Crawford, Jr., Phys. Rev. B **19**, 3217 (1979).
[15] G. P. Summers, G. S. White, K. H. Lee, and J. H. Crawford, Jr., Phys. Rev. B **21**, 2578 (1980).
[16] R. C. DuVarney, A. K. Garrison, J. R. Niklas, and J. M. Spaeth, Phys. Rev. B **24**, 3693 (1981).
[17] B. M. Klein, W. E. Pickett, L. L. Boyer, and R. Zeller, Phys. Rev. B **35**, 5802 (1987).
[18] G. H. Rosenblatt, M. W. Rowe, G. P. Williams, Jr., R. T. Williams, and Y. Chen, Phys. Rev. B **39**, 10309 (1989).
[19] Q. S. Wang and N. A. W. Holzwarth, Phys. Rev. B **41**, 3211 (1990).
[20] A. Stashans, E. Kotomin, and J.-L. Calais, Phys. Rev. B **49**, 14854 (1994).
[21] Y.-N. Xu, Z.-Q. Gu, X.-F. Zhong, and W.-Y. Ching, Phys. Rev. B **56**, 7277 (1997).
[22] E. A. Kotomin and A. I. Popov, Nucl. Instrum. Methods B **141**, 1 (1998).
[23] J. Carrasco, N. Lopez, C. Sousa, and F. Illas, Phys. Rev. B **72**, 054109 (2005).
[24] Y. F. Zhukovskii, E. A. Kotomin, R. A. Evarestov, and D. E. Ellis, Int. J. Quantum Chem. **107**, 2956 (2007).
[25] N. D. M. Hine, K. Frensch, W. M. C. Foulkes, and M. W. Finnis, Phys. Rev. B **79**, 024112 (2009).
[26] P. Rinke, A. Schleife, E. Kioupakis, A. Janotti, C. Rödl, F. Bechstedt, M. Scheffler, and C. G. Van de Walle, Phys. Rev. Lett. **108**, 126404 (2012).
[27] E. Ertekin, L. K. Wagner, and J. C. Grossman, Phys. Rev. B **87**, 155210 (2013).

[28] M. Choi, A. Janotti, and C. G. Van de Walle, J. Appl. Phys. **113**, 044501 (2013).
[29] S. Lany and A. Zunger, Phys. Rev. B **81**, 113201 (2010).
[30] R. Vidya, P. Ravindran, H. Fjellvåg, B. G. Svensson, E. Monakhov, M. Ganchenkova, and R. M. Nieminen, Phys. Rev. B **83**, 045206 (2011).
[31] A. Alkauskas and A. Pasquarello, Phys. Rev. B **84**, 125206 (2011).
[32] A. Malashevich, M. Jain, and S. G. Louie, Phys. Rev. B **89**, 075205 (2014).
[33] A. T. Brant, E. M. Golden, N. C. Giles, S. Yang, M. A. R. Sarker, S. Watauchi, M. Nagao, I. Tanaka, D. A. Tryk, A. Manivannan, and L. E. Halliburton, Phys. Rev. B **89**, 115206 (2014).
[34] P. Deak, B. Aradi, and T. Frauenheim, Phys. Rev. B **92**, 045204 (2015).
[35] H. Nakaya, H. Matsuura, Y. Nakao, S. Shimakawa, M. Goto, S. Nakagawa, and M. Nishikawa, Nucl. Eng. Des. **271**, 505 (2014).
[36] M. Briec, J. J. Abassin, M. Masson, E. Roth, P. Sciers, and H. Werle, J. Nucl. Mater. **155**, 549 (1988).
[37] M. Nishikawa, T. Kinjyo, T. Ishizaka, S. Beloglazov, T. Takeishi, M. Enoeda, and T. Tanifuji, J. Nucl. Mater. **335**, 70 (2004).
[38] M. Oyaidzu, T. Takeda, H. Kimura, A. Yoshikawa, M. Okada, K. Munakata, M. Nishikawa, and K. Okuno, Fusion Sci. Technol. **48**, 638 (2005).
[39] J. Tombrello, H. T. Tohver, Y. Chen, and T. M. Wilson, Phys. Rev. B **30**, 7374 (1984).
[40] R. Pandey and J. M. Vail, J. Phys.: Condens. Matter **1**, 2801 (1989).
[41] M. M. Kuklja, E. V. Stefanovich, E. A. Kotomin, A. I. Popov, R. González, and Y. Chen, Phys. Rev. B **59**, 1885 (1999).
[42] A. Janotti and C. G. Van de Walle, Nat. Mater. **6**, 44 (2007).
[43] M. H. Auvray-Gely, A. Perez, and A. Dunlop, Cryst. Latt. Def. Amorph. Mater. **17**, 119 (1987).
[44] M. H. Auvray-Gely, A. Perez, and A. Dunlop, Philos. Mag. B **57**, 137 (1988).
[45] M. S. Holston, J. W. McClory, N. C. Giles, and L. E. Halliburton, J. Lumin. **160**, 43 (2015).
[46] L. E. Halliburton and L. A. Kappers, Solid State Commun. **26**, 111 (1978).
[47] M. Marezio, Acta Crystallogr. **19**, 396 (1965).
[48] J. Zou, S. Zhou, J. Xu, L. Zhang, Z. Xie, P. Han, and R. Zhang, J. Appl. Phys. **98**, 084909 (2005).
[49] S. Stoll and A. Schweiger, J. Magn. Reson. **178**, 42 (2006).
[50] S. R. Kurtz, D. G. Stinson, H. J. Stapleton, and M. M. Abraham, Phys. Rev. B **24**, 4983 (1981).
[51] D. L. Dexter, Phys. Rev. **101**, 48 (1956).
[52] B. Cockayne and B. Lent, J. Cryst. Growth **54**, 546 (1981).
[53] B. P. Johnson and E. B. Hensley, Phys. Rev. **180**, 931 (1969).
[54] G. Blasse and B. C. Grabmaier, *Luminescent Materials* (Springer-Verlag, Berlin, 1994), Appendix 4, pp. 225–226.
[55] R. H. Bartram and A. M. Stoneham, Solid State Commun. **17**, 1593 (1975).